 DOI: 10.2478/acm-2022-0004

CLASSIFIER SPOT COUNT OPTIMIZATION OF AUTOMATED FLUORESCENT SLIDE SCANNING SYSTEM

ZASTKO LUCIAN[1, 2,*], BERETA MARTIN[3], TIMKO JAROSLAV[2, 4] AND BELYAEV IGOR[1]

[1]Department of Radiobiology, Cancer Research Institute, Biomedical Research Center, University Science Park for Biomedicine, Slovak Academy of Sciences, Bratislava, Slovakia
[2] Department of Laboratory Medicine, Faculty of Health Care, Catholic University in Ružomberok, Ružomberok, Slovakia
[3]Department of Radiological Technology, Faculty of Health Care, Catholic University in Ružomberok, Ružomberok, Slovakia
[4]Department of Clinical Microbiology, Central Military Hospital, Ružomberok, Slovakia

Abstract

Purpose: Ionizing radiation induced foci (IRIF) known also as DNA repair foci represent the most sensitive endpoint for assessing DNA double strand breaks (DSB). IRIF are usually visualized and enumerated with the aid of fluorescence microscopy using antibodies to γH2AX and 53BP1. Although several approaches and software packages were developed for the quantification of IRIF, not one of them was commonly accepted and inter-laboratory variability in the outputs was reported. In this study, the sensitization of Metafer software to counting also small appearing IRIF was validated. **Materials and Methods:** Human lymphocytes were γ-irradiated at a dose of 2 Gy. The cells were fixed at 0.5, 1, 2, and 18 hours post-irradiation, permeabilized and IRIF were immunostained using appropriate antibodies. Cell images were acquired with the automatic Metafer system. Radiation-induced γH2AX and 53BP1 foci were enumerated using either manual counting (JCountPro program) or the Metafer software (after its classifier optimization has been done) and compared. The statistical analysis was performed using One-way ANOVA.

Results: The enumeration of 53BP1, γH2AX foci manually by JCountPro did not statistically significantly differ from the automatic one performed with the optimized Metafer classifier. A detailed step-by-step protocol of this successful optimization is described in this study.

Conclusions: We concluded that the Metafer software after the optimization was efficient in objectively enumerating IRIF, having a potential for usage in clinics and molecular epidemiology.

Keywords: DNA double-strand breaks; DNA repair foci; ionizing radiation.

INTRODUCTION

DNA double-strand breaks (DSB) are the most detrimental type of DNA damage. The cytological manifestation of DSB induced by ionizing radiation (IR) is a formation of so-called ionizing radiation-induced foci (IRIF) which are also referred to as DNA repair foci (1). The IRIF can be microscopically visualized as discrete foci around DSB. A key event in the IRIF formation is the rapid phosphorylation of histone H2AX (γH2AX) that marks a chromatin scaffold formed on a 2 megabase-sized chromatin domain containing DSB. This domain functions by recruiting proteins involved in DSB repair (2). The γH2AX has beco-

Corresponding author: exonzast@savba.sk; lucian.zastko@ku.sk

©2022 Zastko L. et al.
This work is licensed under the Creative Commons Attribution-NonCommercial-NoDerivs 4.0 License (https://creativecommons.org/licenses/by-nc-nd/4.0/)

me a well-established biomarker for IRIF in low-dose research (3), diagnostic radiology (4 – 6), cancer research and therapy (7), and biological dosimetry (8 – 11). Another established molecular marker of DSB is p53 binding protein 53BP1 (12 – 14). Due to different kinetics of formation and decay, γH2AX and 53BP1 foci do not always co-localize (15, 16). However, co-localized γH2AX/53BP1 foci are commonly considered as the most reliable marker for DSB (17, 18).

Several software/freeware programs were developed and used for automatic IRIF scoring in human cell lines (19 – 27). The majority of studies focus on human lymphocyte because these cells are readily available for different purposes. Computational algorithms designed to identify and count foci operate with a certain number of parameters that need to be specified by the user. Recently, the JCountPro software was verified on the same samples in two independent laboratories for enumeration of γH2AX, 53BP1 foci and their co-localization after irradiation of human lymphocytes with low doses (28). The Metafer slide scanning system (MetaSystems, GmbH, Altlussheim, Germany) classifier sensitization to counting small foci (often falsely considered for background noise) and a consequent comparison to manual counting performed using the JCountPro software has been evaluated in this study.

MATERIALS AND METHODS

Reagent grade chemicals were obtained from Sigma-Aldrich (St. Louis, MO, USA), Merck KgaA (Darmstadt, Germany), and Life technologies (Carlsbad, CA). This study has been approved by the Ethics Committee of Children's Hospital in Bratislava. Umbilical cord blood mononuclear cells (UCB MNC), extracted as previously described (29), from three healthy newborns after full-term pregnancies, were provided by Dr. M. Kubes, Eurocord-Slovakia, Bratislava, Slovak Republic.

Frozen UCB MNC were thawed and diluted in 10 ml of thawing medium containing 4.5 ml of Hanks´ Balanced Salt Solution (HBSS) medium (Gibco, Life Technologies, United Kingdom), 1 ml of 1 mg/ml DNAse I Sigma-Aldrich (St. Louis, MO, USA), (100 μg/ml working concentration), and 4.5 ml of Roswell Park Memorial Institute medium (RPMI) 1640 medium with L-glutamine and 4-(2-hydroxyethyl)-1-piperazineethane-sulfonic acid (Hepes) (PAA Laboratories GmbH, Pasching, Austria). Adherent cells (monocytes) were excluded after 2 hour (h) incubation of cells in 25 ml of basal medium (BM): RPMI 1640 medium, supplemented with 10% fetal bovine serum (FBS), 100 IU/ml penicillin, 100 mg/ml streptomycin (Gibco, Invitrogen, Germany). The viability of remaining umbilical cord blood lymphocytes (UCBL) was not less than 95% as defined by the Trypan blue exclusion assay. After 2 h incubation, UCBL were spun down at 100 g, diluted in 50 ml (approximate cell density of $2x10^6$/ml) of BM, and then divided into 2 aliquots (one to be irradiated and one as a control) and incubated on ice 40 min prior to irradiation. UCBL were irradiated by γ-rays at the dose rate of 0.45 Gy/min with a dose of 2 Gy using the cobalt ^{60}Co - TERAGAM® K-02 source (UJP Praha, Prague, Czech Republic). The dose deviation was below 5%. The already irradiated cells were immediately warmed to 37°C (±0.1°C) in a water bath (ED v.2, Julabo Labortechnik GmbH, Seelbach, Germany) and then incubated at 37°C in a humidified incubator (NB-203XL, N-BIOTEK, Inc., Bucheon, South Korea) at 5% CO_2 for 0.5 – 18 h.

0.5, 1, 2, and 18 h post-irradiation, UCBL were washed with a phosphate-buffered saline (PBS, 3.2 mM Na2HPO4, 0.5 mM KH2PO4, 1.3 mM KCl, 135 mM NaCl, pH 7.4) and spun down using the Shandon Double Cytofunnels (ThermoScientific, Runcorn, Cheshire, UK) on the double cytoslides coated with polysine (ThermoScientific, Menzel-Glaser, Braunshweig, Germany) at 85 g, 5 min using the Cellspin I cytocentrifuge (Tharmac GmbH, Germany). The cells were fixed with 3% paraformaldehyde for 15 min and left in the fridge overnight (for 16 – 17 h). The cells were then permeabilized with 0.2% TRITON X-100 for 5 min, washed extensively with PBS, and blocked in 3% FBS (Gibco, Germany) for 30 min at RT.

The primary antibodies, monoclonal γH2AX antimouse (cat. no. #NB100-78356, Novus Biologicals, United Kingdom) (dilution 1:800) and polyclonal 53BP1 antirabbit (cat. no. #NB100-304, Novus Biologicals, United Kingdom) (dilution 1:1000), were diluted in 3% FBS in PBS and applied in 100 µl aliquots to the slides. The slides were incubated for 1 h in a humidified chamber at RT. After washing with PBS, the secondary antibodies, Alexa Fluor 488 IgG (H+L) polyclonal antirabbit (cat. no. #A11029, Invitrogen Molecular Probes, Life Technologies, USA) (dilution 1:200) and Alexa Fluor 555 IgG (H+L) monoclonal antimouse (cat. no. 21429, Invitrogen Molecular Probes, Life Technologies, USA) (dilution 1:200), were added. Then, the slides were incubated for 1 h in the humidified chamber at RT, washed with PBS, and counterstained with an antifade reagent agent VECTASHIELD (Vector Laboratories, Peterborough, United Kingdom) containing 4',6-diamidino-2-phenylindole (DAPI).

Image acquisition of DSB repair foci were conducted using the Metafer Slide Scanning System V 3.9 and Zeiss Axio Imager.Z2 epifluorescent microscope (Carl Zeiss Microscopy GmbH, Gottingen, Germany).

The comparison between groups for pooled data that fitted normal distribution (analyzing designs with a single categorical independent variable) was performed using a One-way ANOVA test, adjusted by Post-hoc Fisher LSD test. All statistical operations were carried out using the Statistica 8.0 software (StatSoft Inc., Tulsa, OK, USA). The results were considered as significantly different at $p < 0.05$.

RESULTS

The „step-by-step“ classifier spot count optimization

One of the focus enumeration problems with the Metafer system is an incomplete small foci counting, which needs to be optimized in order to result transparency, as major portion of small foci are often considered falsely for background noise. We decided to perform this classifier „small foci counting disability repair“ operation on lymphocytes from peripheral blood samples and then check the newly optimized classifier functionality on a comparison of UCBL manually (JCountPro) and by Metafer counted γH2AX and 53BP1 levels induced by 2 Gy γ-irradiation. The creation of the new classifier from an existing one to read the initial settings from was the first thing to perform and the following parameters were checked: correct focus parameter set, correct color channels definition, magnification and microscope configuration. Then the training data, used for the new classifier spot count optimization, were recorded – we chose the experiment performed on lymphocytes from peripheral blood, where small foci were induced as a consequence of 0.1 Gy γ-irradiation (data not shown).

Image quality

The next step in the optimization of the new classifier spot count was to check the image quality with respect to the signal background, signal intensity, and integration time and to define, which objects (cells) we wanted the Metafer to detect (this was done at the training images) (Figure 1A). When processing the images in the Metafer MetaCyte software in the lower right corner of the screen the colored squares representing the available color channels are shown. Within the squares of the color channels used, the integration time is displayed. This value should be checked carefully for different image fields: for images with visible signals it should be lower than the maximum integration time that is defined in the corresponding MetaCyte classifier.

Only in empty images or images not showing signals it should be equal to the maximum integration time. Besides the integration time there was also other thing that needed to be checked – the noise background level of the images. If the noise level is too high (granular background), it is difficult or even impossible to optimize the spot counting. In this case the

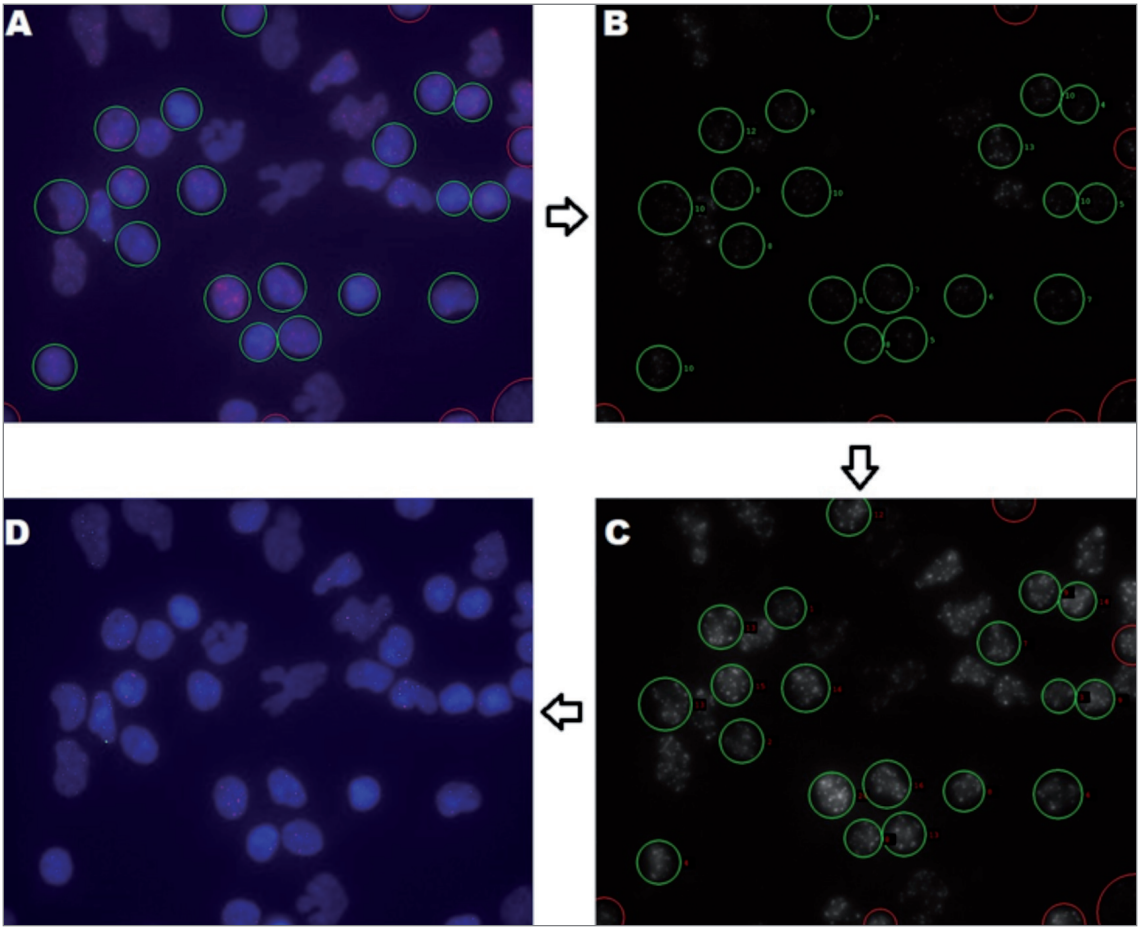


Fig. 1. Training images obtained and processed with the Metafer slide scanning system. A: classifying the cells of interest: green circles – the cell of the right morphology, red circles – rejected cells (image before the application of image processing operations); **B:** green numbers in dark squares as well as white spots inside the green circles represent spot counts of 53BP1 foci for each classified positive cell; **C:** red numbers in dark squares as well as white spots inside the green circles represent spot counts of γH2AX foci for each classified positive cell; **D:** training image obtained after the application of sequence of image processing operations (compare with image A).

camera gain could be lowered. Vice versa, if the background level of the images is low but long integration times have been used, the camera gain could be increased. If very bright artifacts seem to interfere with the integration time adjustment and the signal intensities are poor, the following question arises: if the „*Use Counterstain Mask during Capturing?*“ option of the corresponding MetaCyte classifier has been enabled. In all cases, where a change of the settings for image capturing is needed, the whole re-capture process of the training data, before proceeding with cell classification and adjustment of image processing operations need to be repeated and recorded again. After obtaining properly captured and recorded training images we classified the cells of interest (of right morphology) as well as cells we wanted the Metafer to reject (cells lying at the border of the classified image) and to exclude from analyses (Figure 1B). The number of classified images reached the amount of nearly 50, the number of classified cells within, used for classifier optimization, reached up to 500.

To optimize the classifier on spot counting, the number of spots of the already classified cells needed to be defined first. The best option here is to adjust the spot count for all positive cells (in green circles), for each color channel separately. The selected color channel of the actual image field will be displayed in black and white, where the number of white spots inside the circle equals the number of foci and the spot count can be defined (Figure 1C). If the spot count for a cell cannot be specified (e.g. granular background or low intensity of spots), there is an option to reject it for only this color channel by selecting „**X**" as spot count. In this case the cell will not be used for optimizing the spot count in this color channel.

Image processing operations

To increase the image quality and set a lower threshold, thus order the classifier what should be brought to front and counted, image processing operations can be used. The proper set-up-way for their gain is to open the training data and try out and find the best possible sequence, so-called image processing algorithm, from image processing operations (***Background***, ***Mask***, ***Sharpening***, ***Smoothing***, ***Threshold***, ***Gray Levels***, ***Image Buffers,*** and ***Other***) by applying them to the training images (Figure 1D). Our group, after a careful consideration and countless analyses, decided to use three of them, as these three particularly influenced the overall outcome of the "pre-optimizations" the most – **Background**, **Threshold**, and **Grey Levels**.

- **Background** – By opening this option, the number of all different possible operations is listed. We are using just one of them, *SBLocMinAsy (Subtract background, Local Asymmetric Minimum).* This operation is very efficient in removing a continuous variable background, but produces artifacts if there are discontinuities in the background intensity. If for example the within cell fluorescence background in a signal channel is much higher than the between cell background level, there will be ring shaped artifacts at the nucleus borders. The *SBLocMinAsy* operation avoids this by analyzing the background intensities on all four sides of the current pixel separately and then subtracting the highest of the four values.
- **Threshold** – Here we are making use of *SegThrAbs(X) (Set Absolute Segmentation Threshold at X/1000)* operation that subtracts the segmentation threshold to the specified value. The threshold is specified in units of X/1000 of the available grey level range. To apply the calculated segmentation threshold, where all grey levels less than or equal to the threshold are set to zero, we also chose *ApplySegThr (Apply Current Segmentation Threshold)* operation.
- **Grey levels** – To calculate an upper threshold and then stretch the grey levels between 0 and this threshold to the full available range (0…255), we chose *StretchGL-NSP(X) (Stretch Grey Levels, Number of Saturated Pixels = X)* operation. We set the number of saturated pixels to 10.

Focus parameter set

The number of focus planes of an existing classifier was **7**, the focus plane distance **28/40 µm**, so in order to ensure the scan of the whole cell volume, we increased the number of focus planes of newly created one to **10**, but nothing was changed in the plane distance.

There are 5 parameters for spot counting to be optimized: ***Spot Measurement Area (rel./abs.)***, ***Min. Spot Distance (rel./abs.)***, ***Min. Spot Rel. Intensity (%)***, ***Maximum Spot Area,*** and ***Minimum Spot Contrast***. For the columns ***Min.***, ***Max.***, and ***Step*** it is possible to enter values for all 5 parameters before starting the optimization, the ***N*** values will be updated automatically, the total number of parameter combinations is displayed in the line ***Iteration:***. As all 5 spot counting parameters depend on each other, it is best to optimize them

together. We avoided doing an optimization of multiple parameters with wide ranges and small steps at the same time. It is recommended first to find a preliminary optimum using a wide range, but relatively large steps. Then a second optimization around this parameter combination with small steps can be done to find the optimum parameters more precisely.

- The values of an existing classifier focus parameter set: for FITC (53BP1) signal - *Abs. Spot Meas. Area 20/100 µm; Distance 5/10 µm; Intensity 25%*;
  for SpOrange (γH2AX) signal - *Abs. Spot Meas. Area 20/100 µm; Distance 5/10 µm; Intensity 25%*;
  for fusion signals – *Channel Mask 6; Max. Dist. 5/10 µm*

We did not manipulate with *Abs. Spot Meas. Area* parameter value but we did focus more on *Distance* and *Intensity* parameter values instead. The selected classified training data were analyzed with all possible combinations of parameter values specified by the ranges (for both signals: *Distance 1 – 4/10 µm; Intensity 5 – 20%*) and steps for the single parameters.

- The values of the newly optimized classifier focus parameter set: for FITC (53BP1) signal - *Abs. Spot Meas. Area 20/100 µm; Distance 3/10 µm; Intensity 10%*;
  for SpOrange (γH2AX) signal – *Abs. Spot Meas. Area 20/100 µm; Distance 2/10 µm; Intensity 5%*;
  for fusion signals – *Channel Mask 6; Max. Dist. 5/10 µm*

While the optimization was carried out, several fields were simultaneously updated. In the column ***Best*** the parameter values for the iteration with the smallest error index were displayed. After the first iteration had been finished, the elapsed time and estimated duration of the optimization were displayed. Depending on the size of the training data set, the speed of the computer and the defined number of iterations the classifier optimization would take several hours and therefore had been done overnight.

After the optimization had been finished the values from the column ***Best*** were transferred to the columns ***Min.*** and ***Max.*** and saved. The optimization was performed for all signal channels used for spot counting.

Validation of newly optimized classifier

UCBC used for validation of the newly optimized classifier were isolated from umbilical cord blood of three probands (63, 66, and 67). The cells were exposed to 2 Gy γ-irradiation and then the training images displaying γH2AX and 53BP1 levels were captured and recorded by the automated Metafer Slide Scanning System (Version 3.6) (Figure 2). However, their evaluation was done purposely in two ways: 1. the training images were transferred and each cell γH2AX and 53BP1 levels were manually (by eye) counted in the JCountPro program; 2. the automated counting with the newly optimized Metafer classifier. In both cases there was one main condition obeyed – the application of threshold with respect to background where all grey levels less than or equal to the threshold were set to zero.

The following time points of monitoring the γH2AX and 53BP1 foci levels after the irradiation were carried out: 0.5, 1, 2, and 18 hours. For each time point, foci mean values enumeration of the control as well as irradiated samples, at least 500 UCBC were included into the analyses.

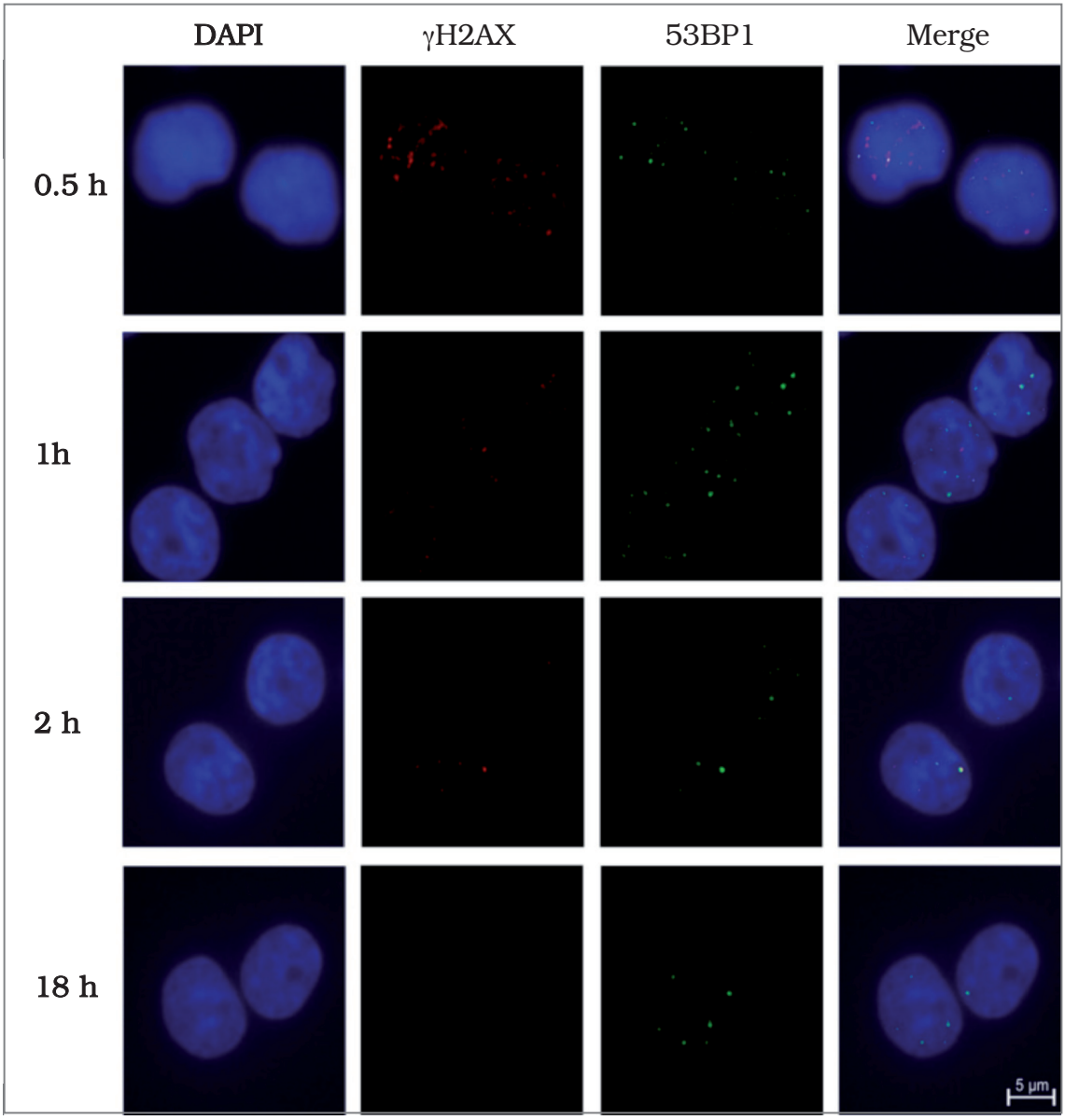


Figure 2. Representative images. The Metafer γH2AX and 53BP1 focus formation in UCBL after γ-irradiation with a radio-therapeutic dose (2 Gy) at different time points after the exposure.

There was no statistically significant difference found between the Metafer and Image Pro γH2AX and 53BP1 foci mean values enumerations, so we could have considered the new classifier for foci counting as successfully optimized. We also assessed the efficiency of our newly optimized classifier, comparing the mean excess foci levels of γH2AX and 53BP1 (Metafer/JCountPro) in UCBL (Figure 3). The assessed efficiency value equaled to 86.3%, which was a success, considering the fact that the efficiency value of our old classifier fluctuated somewhere between 45 – 65%.

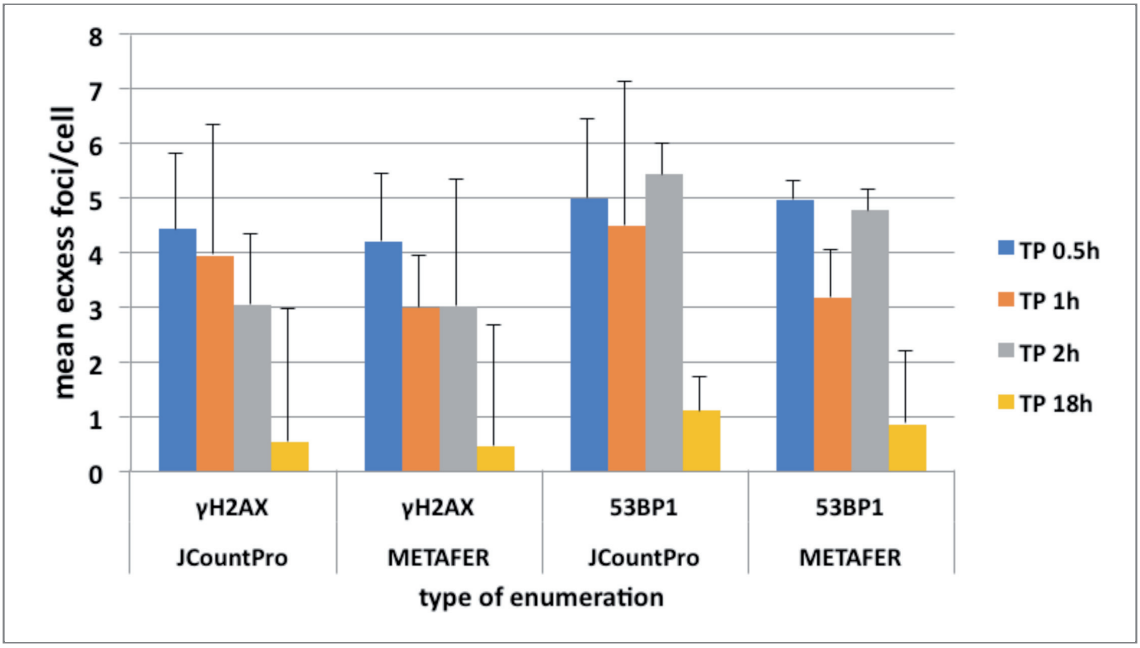


Figure 3. Comparison of the mean excess foci levels of γH2AX and 53BP1. - induced by 2 Gy of γ-irradiation, between the automated newly optimized Metafer system classifier and the manual JCountPro counting in UCBL from three different probands. TP abbreviation stands for time point. The vertical bars represent standard deviations.

DISCUSSION

A real image obtained by using available immunofluorescent staining and confocal microscopy technologies features the presence of the background signal and the variation of the signal in the focus area. The segmentation of such images is usually based on the introduction of the intensity threshold parameter that is present explicitly or implied in majority of focus identification algorithms. The results of the automated focus analysis are highly dependent on the values of the parameters used in a computational approach. Many studies (7, 22, 30) that are based on computational approaches specify the values of these parameters.

According to Qvarnstrom et al. (19) the dependence of the counting results on the chosen parameter values raises the issue of what should be considered as a focus. The results of their study indicate that although the number of automatically counted foci depends on the chosen intensity threshold, the linearity of the dose response is maintained for different threshold values, and therefore it is suggested to use the focus count as a relative measure. This raises the question of how foci counted by an automatic procedure relate to those counted manually and invokes a criticism of automatic focus counting. The simple intensity threshold segmentation also fails to separate two or more adjacent objects (potential foci) if the valley (minimum intensity) between these objects is above the threshold. Another disadvantage of the intensity threshold segmentation is that, due to unavoidable variations between the images in average intensity, individual threshold values need to be applied for various images, and some published algorithms suggest a calculation of individual threshold for each image.

Any computational algorithm designed to identify and count foci operates with a certain number of parameters that need to be specified by the operator. Obviously, algorithms with a smaller number of parameters are preferable since they would be less complicated, easier to learn, and more user friendly. However, there is a certain minimum number of parameters dictated mainly by the quality and complexity of images.

To conclude, the automated focus counting approaches are still evolving with an honest intention to find a reliable, uncomplicated, and at last but not least affordable computational approach.

REFERENCES

1. Bekker-Jensen S, Lukas C, Kitagawa R, Melander F, Kastan MB, Bartek J, Lukas J. 2006. Spatial organization of the mammalian genome surveillance machinery in response to DNA strand breaks. J Cell Biol.173:195 – 206.
2. Rogakou EP, Boon C, Redon C, Bonner WM. 1999. Megabase chromatin domains involved in DNA double-strand breaks in vivo. J Cell Biol. 146:905 – 916.
3. Rothkamm K, Löbrich M. 2003. Evidence for a lack of DNA double-strand break repair in human cells exposed to very low X-ray doses. Proc Natl Acad Sci USA. 100:5057 – 5062.
4. Rothkamm K, Balroop S, Shekhdar J, Fernie P, Goh V. 2007. Leukocyte DNA damage after multidetector row CT: a quantitative biomarker of low-level radiation exposure. Radiology. 242:244 – 251.
5. Depuydt J, Baert A, Vandersickel V, Thierens H, Vral A. 2013. Relative biological effectiveness of mammography X-rays at the level of DNA and chromosomes in lymphocytes. Int J Radiat Biol. 89:532 – 538.
6. Vandevoorde C, Gomolka M, Roessler U, Samaga D, Lindholm C, Fernet M, Hall J, Pernot E, El-Saghire H, Baatout S, et al. 2015. EPI-CT: in vitro assessment of the applicability of the gamma-H2AX-foci assay as cellular biomarker for exposure in a multicentre study of children in diagnostic radiology. Int J Radiat Biol. 91:653 – 663.
7. Ivashkevich AN, Martin OA, Smith AJ, Redon CE, Bonner WM, Martin RF, Lobachevsky PN. 2011. gammaH2AX foci as a measure of DNA damage: a computational approach to automatic analysis. Mutat Res. 711:49 – 60.
8. Barnard S, Ainsbury E, Al-Hafidh J, Hadjidekova V, Hristova R, Lindholm C, Gil OM, Moquet J, Moreno M, Rößler U. 2014. The first gamma- H2AX biodosimetry intercomparison exercise of the developing European biodosimetry network RENEB. Radiat Protect Dosimetry. ncu259.
9. Lamkowski A, Forcheron F, Agay D, Ahmed EA, Drouet M, Meineke V, Scherthan H. 2014. DNA damage focus analysis in blood samples of minipigs reveals acute partial body irradiation. Plos One. 9:e87458.
10. Viau M, Testard I, Shim G, Morat L, Normil MD, Hempel WM, Sabatier L. 2015. Global quantification of cH2AX as a triage tool for the rapid estimation of received dose in the event of accidental radiation exposure. Mutat Res/Genet Toxicol Environ Mutagenesis. 793:123 – 131.
11. Jakl L, Marková E, Koláriková L, Belyaev I. 2020. Biodosimetry of Low Dose Ionizing Radiation Using DNA Repair Foci in Human Lymphocytes. Genes (Basel). Jan 4; 11(1):58.
12. Horn S, Barnard S, Rothkamm K. 2011. Gamma-H2AX-based dose estimation for whole and partial body radiation exposure. PLoS One. 6:e25113.
13. Wojewodzka M, Sommer S, Kruszewski M, Sikorska K, Lewicki M, Lisowska H, Wegierek-Ciuk A, Kowalska M, Lankoff A. 2015. Defining blood processing parameters for optimal detection of gamma-H2AX foci: a small blood volume method. Radiat Res. 184:95 – 104.
14. Zastko L, Petrovičová P, Račková A, Jakl L, Jakušová V, Marková E, Belyaev I. 2021. DNA damage response and apoptosis induced by hyperthermia in human umbilical cord blood lymphocytes. Toxicology in Vitro. Volume 73. 105127, ISSN 0887-2333.
15. Markova E, Schultz N, Belyaev IY. 2007. Kinetics and dose-response of residual 53BP1/gamma-H2AX foci: co-localization, relationship with DSB repair and clonogenic survival. Int J Radiat Biol. 83:319 – 329.

16. Groesser T, Fontenay GV, Han J, Chang H, Pluth J, Parvin B. 2015. Quantification of the dynamics of DNA repair to ionizing radiation via colocalization of 53BP1 and gamma H2AX. In: Bhanu B, Talbot P, editors. Video bioinformatics: from live imaging to knowledge: Computational Biology Series, v. 22: Dordrecht: Springer. p. 253 – 263.
17. Vandevoorde C, Gomolka M, Roessler U, Samaga D, Lindholm C, Fernet M, Hall J, Pernot E, El-Saghire H, Baatout S, et al. 2015. EPI-CT: in vitro assessment of the applicability of the gamma-H2AX-foci assay as cellular biomarker for exposure in a multicentre study of children in diagnostic radiology. Int J Radiat Biol. 91:653 – 663.
18. Zastko L, Račková A, Petrovičová P, Durdík M, Míšek J, Marková E, Belyaev I. 2021. Evaluation of Calyculin A Effect on γH2AX/53BP1 Focus Formation and Apoptosis in Human Umbilical Cord Blood Lymphocytes. Int J Mol Sci. 22(11):5470.
19. Qvarnstrom OF, Simonsson M, Johansson KA, Nyman J, Turesson I. 2004. DNA double strand break quantification in skin biopsies. Radiother Oncol. 72:311 – 317.
20. Bocker W, Iliakis G. 2006. Computational methods for analysis of foci: validation for radiation-induced gamma-H2AX foci in human cells. Radiat Res. 165:113 – 124.
21. Barber P, Locke R, Pierce G, Rothkamm K, Vojnovic B. 2007. Gamma- H2AX foci counting: image processing and control software for highcontent screening: Biomedical Optics (BiOS) 2007:64411M–64411M-10.
22. Hou Y-N, Lavaf A, Huang D, Peters S, Huq R, Friedrich V, Rosenstein BS, Kao J. 2009. Development of an automated c-H2AX immunocytochemistry assay. Radiat Res. 171:360 – 367.
23. Roch-Lefevre S, Mandina T, Voisin P, Gaetan G, Mesa JE, Valente M, Bonnesoeur P, Garcia O, Voisin P, Roy L. 2010. Quantification of gamma-H2AX foci in human lymphocytes: a method for biological dosimetry after ionizing radiation exposure. Radiat Res. 174:185 – 194.
24. Turner HC, Sharma P, Perrier JR, Bertucci A, Smilenov L, Johnson G, Taveras M, Brenner DJ, Garty G. 2014. The RABiT: high-throughput technology for assessing global DSB repair. Radiat Environ Biophys. 53:265 – 272.
25. Kosik P, Durdik M, Jakl L, Skorvaga M, Markova E, Vesela G, Vokalova L, Kolariková L, Horvathova E, Kozics K, Belyaev I. 2020. DNA damage response and preleukemic fusion genes induced by ionizing radiation in umbilical cord blood hematopoietic stem cells. Sci Rep. 10. 13722.
26. Misek J, Laukova T, Kohan M, Veternik M, Jakusova V, Jakus J. 2018.Measurement of Low-level radiofrequency electromagnetic fields in the human environment. Acta Medica Martiniana. 18(2): 27 – 33.
27. Sladicekova K, Bereta M, Misek J, Parizek D, Jakus J. 2021. Biological effects of a low-frequency electromagnetic field on yeast cells of the genus Saccharomyces Cerevisiae. Acta Medica Martiniana. 21(2): 34 – 41.
28. Jakl L, Lobachevsky P, Vokálová L, Durdík M, Marková E, Belyaev I. 2016. Validation of JCountPro software for efficient assessment of ionizing radiation-induced foci in human lymphocytes. Int J Radiat Biol. 92(12):766 – 773.
29. Vasilyev SA, Kubes M, Markova E, Belyaev I. 2013. DNA damage response in CD133 + stem/progenitor cells from umbilical cord blood: low level of endogenous foci and high recruitment of 53BP1. Int J Radiat Biol. 89:301 – 309.
30. Cai Z, Vallis KA, Reilly RM. 2009. Computational analysis of the number, area and density of gamma-H2AX foci in breast cancer cells exposed to (111) In-DTPAhEGF or gamma-rays using Image-J software. Int J Radiat Biol. 85:262 – 271.

Acknowledgements
This study was funded by the Slovak Research and Development Agency, Grant number: APVV 15 0250; the IAEA Research Contract MEDBIODOSE No: 24714 and the Operational Programme Integrated Infrastructure for the project: Long-term strategic research of prevention, intervention and mechanisms of obesity and its comorbidities, IMTS: 313011V344, co-financed by the European Regional Development Fund.

Received: February 1, 2022
Accepted: February 24, 2022